

UC San Diego

Independent Study Projects

Title

Genomic correlates of MRI contrast enhancement in glioblastoma

Permalink

<https://escholarship.org/uc/item/3s46r1nk>

Author

Treiber, Jeffrey M.

Publication Date

2017

Independent Study Project

University of California, San Diego

Title of Project: Genomic correlates of MRI contrast enhancement in glioblastoma
Author: Jeffrey M. Treiber

Abstract

In magnetic resonance imaging (MRI) gadolinium-based contrast agents are administered to identify areas of blood brain barrier compromise that result in brain tumor enhancement¹. The most common primary brain tumor, glioblastoma, is characterized on MRI by its heterogeneous uptake of gadolinium contrast². Both the heterogeneity and magnitude of contrast enhancement helps clinicians to distinguish glioblastoma from other primary brain tumors³ as well as intracranial metastases⁴. Unfortunately, the precise molecular mechanisms which govern unique patterns of contrast enhancement remain poorly understood. Furthermore, It has been observed that glioblastoma tumors demonstrate widely different imaging characteristics and degrees of contrast enhancement. Previous studies have demonstrated relationships between contrast enhancement and overall survival as well as tumor gene expression of pathways related to cell division and hypoxia⁵. However, these studies were limited by small sample sizes⁵ and coarse qualitative metrics⁵⁻⁹.

Using The Cancer Imaging Archive (TCIA), a method of automated segmentation developed by our laboratory¹⁰, and matched tumor genomic data from The Cancer Genome Atlas (TCGA) this study examined the genomic correlates of quantitative measures of contrast enhancement (CE). Metrics for contrast enhancement included relative CE (rCE), CE heterogeneity, and ratio of total CE volume to the volume of the filled CE ring (CE:CEfilled). Analyses revealed relationships between rCE and inflammation, CE heterogeneity and angiogenesis, and CE:CEfilled with cell division. Age-adjusted cox regression found a significant overall survival benefit to patients with higher CE heterogeneity (HR = 0.36, p < 0.01).

Uncovering relationships between contrast enhancement and genomics may better characterize glioblastomas and improve the understanding of its pathophysiology, which may lead to future therapies and better patient care.

Introduction

Glioblastoma is the most common primary brain tumor¹¹. With a median survival of 12-14 months¹², this malignancy is notorious for its resistance to chemotherapy and radiotherapy, and recurrence after surgical resection. Glioblastoma demonstrates a predilection to invade local tissue and rapidly accumulate adaptive mutations to outlast aggressive care including surgical resection, chemotherapy, and radiation¹³. Histologically, Glioblastoma is differentiated from lower grade astrocytomas by microvascular proliferation and the presence of tissue necrosis¹⁴. In neuroimaging, glioblastoma is often

characterized as a large mass composed of a thick, irregularly shaped contrast enhancing borders with central necrosis surrounded by vasogenic edema². Despite this characterization however, the appearance of glioblastoma on MR imaging varies broadly, and tumors can be multi-focal, cystic, thin ringed, or contain large portions of non-enhancing tumor². The underlying genetic mechanisms that relate to these vastly different radiophenotypes have yet to be fully elucidated¹⁵.

Contrast enhancement is of particular interest as it is used for the initial work up for patients with a suspected intracranial mass and can be utilized for surgical planning and monitoring treatment response. The magnitude and quality of contrast enhancement, for example, can allow differentiation from lower grade gliomas³ and intracranial metastases⁴. Contrast studies can be used to monitor recurrence, evaluate the effectiveness of therapy¹⁶⁻²⁰, or even be used as a prognostic indicator²¹⁻²³.

Abnormal contrast enhancement is fundamentally due to increases in blood brain barrier permeability or blood flow¹. In glioblastoma, this is believed to be caused by tumor angiogenesis that results in local disruption of the blood-brain barrier^{1,24}. Therefore areas of enhancement are believed to represent the areas of greatest metabolic activity while the necrotic core is made up of tumor that has exceeded its available blood supply²⁴.

Previous genomic studies have found associations between contrast enhancement and gene expression of several pathways involved with cellular division, hypoxia, and angiogenesis⁵. These studies were limited however by qualitative metrics using manual measurements and subjective assessments⁵⁻⁹. This study will aim to improve upon previous studies by employing quantitative metrics of contrast enhancement in a large population of patients with complimentary neuroimaging and genomic expression data in order to identify genetic associations of contrast enhancement on MR imaging.

Methods

Imaging preprocessing: Pre-operative MR images from 196 glioblastoma patients from The Cancer Imaging Archive (TCIA; <http://cancerimagingarchive.net>) were downloaded in June 2014 and preprocessed according to pipeline described previously¹⁰. Briefly, images were corrected for gradient field non-linearity, bias-fields, and then registered to Montreal Neurological Institute (MNI) 152 nonlinear 1mm³ template using an affine transform. Inclusion criteria include one artifact-free, pre-operative T1-weighted MRI scan with contrast (T1C).

Using Iterative Probabilistic Voxel Labeling (IPVL), a method of automated segmentation developed by our laboratory¹⁰, the MR images were segmented into five tissue components: contrast enhancing tumor, FLAIR hyperintensity, non-tumor contrast enhancement, gray matter, and white matter. A sixth component consisting of necrosis/cystic material/non-enhancing tumor were generated by filling the inside of the contrast enhancing tumor (CEfilled).

Contrast enhancement parameters: In order to adjust for signal variations between scanner and contrast administration protocols, the T1-weighted image with contrast (T1C) were

normalized by the median intensity of the confluence of the sinuses (Figure 1). This relative contrast enhancement (rCE) was calculated for each contrast enhancing tumor segmentation. In an effort to understand the radiogenomic relationships with CE heterogeneity we quantified heterogeneity by calculating the Shannon entropy²⁵, an intensity independent measure of data complexity of the entire CE segmentation. A third measure was calculated by taking the ratio of contrast enhancing segmentation volume to volume of the CEfilled segmentation (CE:CEfilled). Regions of non-contrast enhancing tumor outside the filled ring were excluded due to the limitations in detection on T1-weighted images and absence of available T2-weighted images. Four examples are shown in Figure 2.

Genomic data: Level 3 probe collapsed, median normalized messenger RNA (mRNA) expression data (affymetrix HG U133A array) was downloaded for a subset of 165 subjects using the TCGA Data portal in June 2014. Differential gene expression was performed for each imaging parameter using a median cut-off. Genes with at least a 1.2 fold-change and a benjamini-hochberg corrected $p < 0.05$ were considered significant. Gene ontology and functional annotation was performed using the Database for Annotation, Visualization, and Integrated Discovery^{26,27} (DAVID; <https://david.ncifcrf.gov/>). Enrichment scores of each signature were calculated for each subject in the TCGA cohort using single sample gene set enrichment analysis²⁸ (ssGSEA). Normalized enrichment scores (NES) were calculated by performing 10,000 permutations.

Results

Differential gene expression of imaging parameters displayed significant enrichment in pathways implicated in tumor biology and inflammation. Mean rCE demonstrated an enrichment of genes associated with inflammation including cytokine production, complement activation, natural killer cell mediated cytotoxicity, lymphocyte activation, and neutrophil chemotaxis (Table 1) while lower mean rCE was associated increased expression of genes associated with DNA repair and checkpoint activation (Table 1). CE heterogeneity was associated with increased expression of genes involved in angiogenesis (VEGFC, IGF1R, and FOS), histones, and neurodevelopment (Table 1). Decreased CE heterogeneity was not associated with significant enrichment for any known pathways. Increased CE:CEfilled ratio displayed increased expression of genes associated with cell division, chromosome condensation, and transcription (Table 1) while there were no known pathways significantly associated with decreased CE:CEfilled.

Normalized enrichment scores of mean rCE and CE entropy gene signatures were not significantly different between subjects in the TCIA cohort and that of the remaining subjects of the TCGA. However, there was a significant decrease in CE:CEfilled NES of the TCIA subjects when compared with the TCGA subjects without imaging ($p = 0.01$).

Age-adjusted cox-proportional hazard model revealed a significant overall survival benefit with increased CE heterogeneity ($HR = 0.36$, $p < 0.01$) but not rCE mean ($p = 0.53$) or CE:CEfilled ($p = 0.86$). There were no significant associations between survival and NES for the gene signatures of the three imaging parameters when applied to all TCGA subjects.

Discussion

Contrast enhancement in MRI is due to extravasation of contrast into the interstitial spaces and increased flow of contrast agents through vessels¹. Contrast enhancement in tumors are believed to be attributable to the formation of immature porous blood vessels in addition to an increase in vascular permeability due to inflammation¹. In our study, we found that our imaging metrics represented different aspects of tumor biology. We found that the magnitude of contrast enhancement normalized to the intensity of contrast within the confluence of the sinuses, to be strongly associated with the expression of genes associated with inflammation. Interestingly, decreased rCE was associated DNA damage repair pathways, which could explain in part, the known radiation resistance of a subpopulation of glioblastoma tumors²⁹. CE heterogeneity, believed to represent degree of angiogenesis through the creation of vessels of varying caliber, displayed enrichment with genes associated with angiogenesis, particularly IGF-1 receptor and VEGFC. A previous study found that CE to necrosis ratios have been associated with increased expression of genes KLK3, IL7R, RBP4, RUNX3, and MS4A1⁵. We did not find increased expression with the genes described in that study but found genes enriched in cellular proliferation pathways, consistent with the understanding that enhancing portions of tumor represent areas of metabolically active tumor. We found that increased CE heterogeneity was associated with greater overall survival. Although CE heterogeneity is associated with angiogenesis, we demonstrate these tumors have a better prognosis. This association could be due to a reliance on more immature blood vessels for supply and may not have the immune privilege afforded to them by a properly formed blood brain barrier. It is also possible that these tumors are in a pro-angiogenic state to compensate for growth resulting in chronic metabolic outpacing.

To see whether the contrast parameters associated gene signatures were generalizable to the rest of the TCGA we compared their enrichment in both cohorts. We should expect that imaging associated signatures should not vary with respect to the TCGA as a whole as the TCIA should represent a subset. We found no difference between the enrichment scores of rCE and CE entropy, however, there was a significant difference with respect to the CE:CEfilled signature enrichment.

Due diligence was performed to ensure that the measures selected for this study would be as unaffected as possible by differences in MR scanners, sequences, and contrast protocols. However, one limitation to this study is that it is currently unknown how these imaging parameters change between site and they should be validated in an additional dataset. Additionally, scan time relative to contrast delivery and contrast dose can vary at institutions. Our method attempted to normalize for the amount of contrast present in the torcula, but scan time relative to contrast injection is a difficult measure to control for and may contribute to inter-institutional differences. Finally, further studies in other cohorts could help better elucidate the pathophysiological mechanisms of contrast enhancement in glioblastoma subjects.

Conclusions

The glioblastoma radiographic parameters of contrast enhancement had significant relationships with angiogenesis, cellular proliferation, and inflammation. Increased contrast enhancement heterogeneity was associated with improved survival. This study has demonstrated that novel

contrast enhancement radiographic parameters can be used to better characterize and understand glioblastoma.

Figures

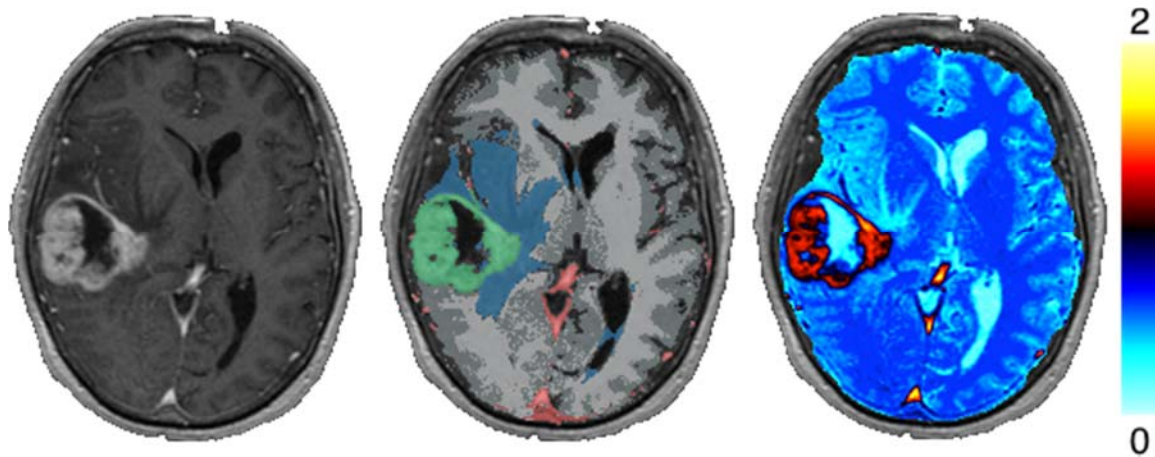


Figure 1. Example segmentation and rCE calculation. T1 with contrast (left). Segmentation (middle) with CE tumor (green), FLAIR hyperintensity (blue), non-tumor contrast enhancement (red), grey matter (grey), white matter (light grey). Relative CE map (left).

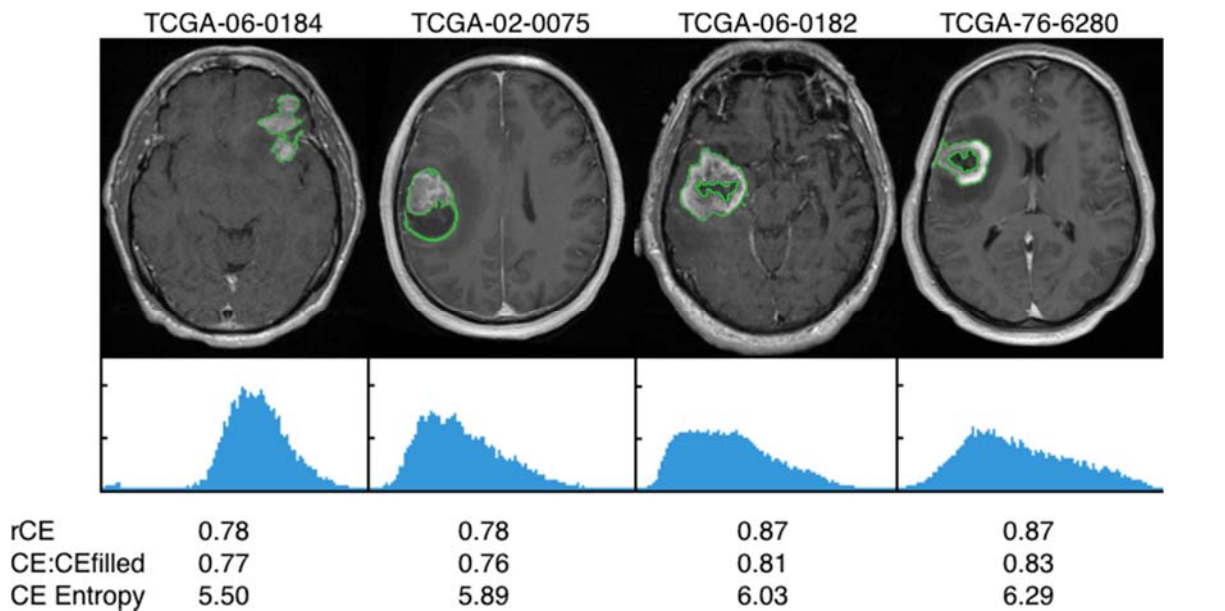


Figure 2. Example subjects demonstrating their CE segmentations (green outline) and imaging parameters (bottom). Visualization of the CE intensity heterogeneity (entropy) is shown as intensity histograms (blue).

Pathway	<i>p</i>	Genes
Relative Contrast Enhancement: Increased		
GO:0006954~inflammatory response	< 0.001	C3AR1, S100A8, AIF1, C3, CCR1, IL18, LY86, TLR1, S100A9, TLR2, FPR1, ITGB2, PF4, TLR5, TLR7, FOLR2, AOA, PYCARD, SYK, CSF1R, BLNK, PLP1, LIPA, LY96, HCK, LYZ, LGALS9, CYBA, CCR5, STAB1, CLEC7A, CD14
Glycoprotein	< 0.001	CADM3, ADORA3, GABRB1, TLR1, TLR2, TLR5, CD53, TLR7, MOG, SLC7A7, SLC2A5, EBI3, INA, F12, CLCA4, PTPRN, LILRB1, C1QA, C1QB, CD37, NPC2, F5, CCR5, CD33, ST14, RELN, CHGB, IBSP, IL1R2, C3AR1, ENPP2, APOC2, IFI30, ITGB2, SLC29A3, FOLR2, SRGN, CSF1R, MGAT4A, GABRA2, CHI3L2, SLAMF8, KCNK1, SLCO2B1, SERPINI1, GPR37, CD300A, CLEC7A, LY86, UCHL1, GPR88, HPSE, EVI2A, AOA, CREG1, SV2B, EVI2B, FCGR3B, LAIR1, LY96, CD163, SIGIRR, CHGA, ADRB2, CD86, FOLH1, GRM3, SIGLEC7, CTSC, TREM2, CTSH, TF, C3, CCR1, GPR65, FPR1, NPTX1, ACSL1, SYN1, IL10RA, FCGR1A, RNASET2, LEFTY2, LY6H, CD4, C2, NEFL, B4GALNT1, KLK6, PTPRC, LIPA, RNASE2, SLC12A5, RNASE6, CPVL, P2RY13, STAB1, CDH19, FCGR2A, CD14
IPR001452:Src homology-3 domain	< 0.001	SH3GL3, FYB, DOCK2, NCF1, HCLS1, HCK, PLCG2, MYO1F, SAMSN1, BIN1, SH3GL2, BTK, SLA, AMPH
Secreted	< 0.001	S100A8, IL18, LY86, S100A9, SNCA, HAMP, HPSE, AOA, CREG1, CFD, FCGR3B, EBI3, F12, CLCA4, LY96, GNLY, LYZ, CD163, LILRB1, C1QA, C1QB, CHGA, NPC2, F5, RELN, TREM2, CHGB, IBSP, IL1R2, TF, CCK, ENPP2, C3, APOC1, IFI30, APOC2, PF4, FOLR2, RNASET2, LEFTY2, C2, SRGN, HAPLN2, KLK6, MGAT4A, RNASE6, CHI3L2, SERPINI1, LGALS9, NPY, SST, CD14

Membrane	< 0.001	CADM3, ADORA3, S100A8, AQP9, AIF1, GABRB1, SNCA, S100A9, TLR1, TLR2, CD53, TLR5, MOG, TLR7, SLC7A7, BTK, SLC2A5, FAM49B, SYK, SH3GL3, CLCA4, NCF1, STMN2, FA2H, BASP1, PTPRN, IGSF6, LILRB1, LHFPL2, CD37, CCR5, VAMP8, CD33, ST14, LILRB4, CX3CR1, VSIG4, BIN2, SH3GL2, C3AR1, IL1R2, LST1, GNAI1, ENPP2, NINJ2, HMP19, ITGB2, FXYP7, CAMKV, PPP1R16B, SLC29A3, DOCK2, LAPTM5, FOLR2, FCER1G, SLC31A2, BLNK, CSF1R, TYROBP, MGAT4A, TESC, GABRA2, FBXO2, SLAMF8, SLCO2B1, KCNK1, RAB33A, CORO1A, RGS1, RGS2, GPR37, UCP2, CD300A, CLEC7A, UCHL1, SPI1, LTC4S, ARHGAP15, GPR88, SYNGR2, RTN2, MBP, EVI2A, HPSE, HMOX1, EVI2B, SV2B, FCGR3B, RHOG, LAIR1, DHRS9, TRPM2, SIGIRR, CD163, EPB41L3, GRM3, CHGA, DHRS3, ADRB2, CD86, FOLH1, SIGLEC7, LRMP, TREM2, CCR1, FPR1, GPR65, APBB1IP, AMPH, PGBD5, ACSL1, IL10RA, ALOX5AP, FCGR1A, LY6H, CD4, MS4A6A, B4GALNT1, MS4A4A, PTPRC, PLP1, TBXAS1, HCLS1, HCK, SLC12A5, MAL, RCAN2, P2RY13, CYBA, PDE2A, STAB1, CDH19, FCGR2A, TMEM176B, CD14, TMEM176A, MGST2
Tuberculosis	< 0.001	C3, IL18, TLR1, TLR2, ITGB2, CORO1A, IL10RA, FCGR1A, FCER1G, FCGR2A, CLEC7A, FCGR3B, CD14, SYK
Lysosome	< 0.001	RNASE2, LIPA, HCK, SNCA, IFI30, TLR7, TRPM2, ADRB2, LAPTM5, NPC2, HPSE, RNASET2, CTSC, CTSB
IPR013151:Immunoglobulin	< 0.001	LILRB1, IL1R2, CD33, FCGR1A, LILRB4, CD4, CSF1R
hsa05150:Staphylococcus aureus infection	< 0.001	C1QA, C3AR1, C1QB, C3, FCGR1A, FPR1, ITGB2, FCGR2A, C2, CFD, FCGR3B
Relative Contrast Enhancement: Decreased		
DNA damage	< 0.001	MSH2, LIG1, SMC5, PRKDC, HERC2, RBBP6, SMC3, CDK2, ATM, EYA4, PAXIP1, RFW3, TIMELESS, BAZ1B, FANCI, MDC1, SUPT16H, USP10, GADD45A, PMS1, FEN1, BARD1

Transcription	< 0.001	ZNF83, ZNF532, YLPM1, ZXDC, RORA, ZEB1, PNN, MAP3K7, ESF1, CASP8AP2, ZNF148, TARDBP, RTF1, BRD7, PSIP1, DDX21, RBBP4, POLR1E, HMG20A, SPEN, MED13, ZNF334, CCNL2, EYA4, TAF12, BAZ1B, TIMELESS, ASCC2, MED17, NCOA6, MGA, MED1, BCLAF1, HMGB2, SOX5, TRIB3, TRRAP, ZNF654, MEIS1, ZNF175, CHD9, CDYL, DDX3X, NFAT5, PER1, LIMD1, ARNTL2, TFD1, HIP1, ZNF263, KLF6, KLF7, ATAD2, WHSC1, ILF3, TFCP2, SMAD1, ZNF665, ZBTB43, NOTCH1, PAXIP1, PHF2, ZNF211, SMARCC1, SUPT16H, ZNF318, NFIB
GO:0005524~ATP binding	< 0.001	BTA1, PRPF4B, FGFR3, ALDH18A1, BLM, UBE2G2, OAS3, TRIB3, CASK, PRKDC, CLK1, TRIB2, TRIB1, MAP3K7, CHD9, MCM7, DHX38, DDX3X, DDX19A, CLK4, PIK3CA, DDX21, ACSL3, PMS1, KIF14, SMCHD1, MSH2, LIG1, SMC5, TPX2, ATAD2, TRIO, ACLY, CCT6A, MCM3, MCM4, SMC3, ATM, CDK2, WEE1, SMC4, MYO10, BAZ1B, SCYL2, SMARCA5, PAICS
Cell cycle	< 0.001	PRC1, KNTC1, MCM7, NIPBL, CASP8AP2, FANCI, MDC1, NCAPG2, BRD7, CLASP1, TPR, ZWILCH, CCNA2, TFD1, STAG1, RBBP4, NASP, LIG1, SMC5, TPX2, CENPF, GAS1, MCM3, MCM4, SMC3, ATM, CDK2, WEE1, SEPT11, SMC4, CDC25B, TIMELESS, GADD45A
GO:0006695~cholesterol biosynthetic process	< 0.001	SQLE, HMGCR, CYP51A1, DHCR7, INSIG1, HMGCS1, ACLY
GO:0005913~cell-cell adherens junction	0.002	LIMA1, PDLIM5, DAG1, EIF2S3, EIF4G1, TJP1, ITGA6, MACF1, DDX3X, EIF4H, ERC1, PAICS, GOLGA3, EPN2
Contrast Enhancement Heterogeneity: Increased		
Ubl conjugation	< 0.001	HIST1H2AC, HIST1H2BD, HIST1H2AE, NFKBIA, HOXC10, FOS, IGF1R, TCERG1, HOXC11, HIST1H2BK, HIST2H2BE, ZMIZ1, MDM2
Transcription regulation	< 0.001	EGR1, ZNF274, JARID2, ZIC1, TCF7L1, HOXC10, HOXA2, TCERG1, HOXC11, HOXA4, ZMIZ1, ZNF395, ZSCAN18, BCOR
Developmental protein	< 0.001	HOXC10, VEGFC, SHROOM2, HOXA2, DACT1, HOXC11, HOXA4, JARID2, ZIC1
GO:0045944~positive regulation of transcription from RNA polymerase II promoter	0.03	EGR1, FOS, HOXA2, HOXC11, ZMIZ1, NFKBIA, ZIC1

hsa05215:Prostate cancer	0.002	IGF1R, NFKBIA, MDM2, TCF7L1
CE to CEfilled ratio: Increased		
		ZNF536, BTAF1, ZNF83, ZNF292, BACH2, ZBTB11, MXI1, ZNF331, ZNF652, TMF1, PLAGL1, NR1D2, ZNF223, ZNF248, HIST3H2A, BAZ2B, ZNF266, NKRF, ZNF43, EGR3, ZNF264, SMAD7, ZFP30, ZNF91, EMX2, ZNF337, TOX3, ATM, SHOX2, RLF, TCFL5, DMTF1, MTF2, ZNF692, ZNF136, DENND4A, ZNF432, ZNF587, ZNF571, REV3L
DNA-binding	0.014	CCNB1IP1, USP6, HERC5, UBR2, HERC2, ASB13, HERC1, KLHL3,
Ubl conjugation pathway	0.038	RAB40B, WSB1, TRIM2, FBXW7, DCUN1D1, UBR5, USP46, PELI2, DIXDC1, MYRIP, EPB41L1, MYO6, ACTN2, DAAM1, ADD3, STK38L,
Actin-binding	0.011	KLHL3, MYO5C
Cell division and chromosome partitioning / Cytoskeleton	0.025	SEPT4, HERC5, HERC2, HERC1
Guanine-nucleotide releasing factor	0.015	RASGRP1, RAPGEF6, RAPGEF4, DENND4A, HERC1, DOCK3, NET1

Table 1. Largest pathway (by number of genes) for each significant DAVID annotation cluster for each imaging parameter.

References

1. Smirniotopoulos, J. G., Murphy, F. M., Rushing, E. J., Rees, J. H. & Schroeder, J. W. Patterns of contrast enhancement in the brain and meninges. *Radiographics* **27**, 525–551 (2007).
2. Rees, J. H., Smirniotopoulos, J. G., Jones, R. V. & Wong, K. Glioblastoma multiforme: radiologic-pathologic correlation. **16**, 1413–38– quiz 1462–3 (1996).
3. Asari, S. *et al.* Assessment of the pathological grade of astrocytic gliomas using an MRI score. *Neuroradiology* **36**, 308–310 (1994).
4. Asari, S. *et al.* Evaluation of MRI score in the differentiation between glioblastoma multiforme and metastatic adenocarcinoma of the brain. *Acta Neurochir (Wien)* **122**, 54–59 (1993).
5. Jamshidi, N., Diehn, M., Bredel, M. & Kuo, M. D. Illuminating radiogenomic characteristics of glioblastoma multiforme through integration of MR imaging, messenger RNA expression, and DNA copy number variation. *Radiology* **270**, 1–2 (2014).
6. Carrillo, J. A. *et al.* Relationship between tumor enhancement, edema, IDH1 mutational status, MGMT promoter methylation, and survival in glioblastoma. *AJNR Am J Neuroradiol* **33**, 1349–1355 (2012).
7. Pope, W. B. *et al.* Relationship between gene expression and enhancement in glioblastoma multiforme: exploratory DNA microarray analysis. *Radiology* **249**, 268–277 (2008).
8. Diehn, M. *et al.* Identification of noninvasive imaging surrogates for brain tumor gene-expression modules. *Proc. Natl. Acad. Sci. U.S.A.* **105**, 5213–5218 (2008).
9. Wang, K. *et al.* Radiologic Features and Expression of Vascular Endothelial Growth Factor Stratify Survival Outcomes in Patients with Glioblastoma. *AJNR Am J Neuroradiol* (2015). doi:10.3174/ajnr.A4567
10. Steed, T. C. *et al.* Iterative Probabilistic Voxel Labeling: Automated Segmentation for Analysis of The Cancer Imaging Archive Glioblastoma Images. (2014). doi:10.3174/ajnr.A4171
11. Ostrom, Q. T. *et al.* CBTRUS Statistical Report: Primary Brain and Central Nervous System Tumors Diagnosed in the United States in 2008-2012. *Neuro-Oncology* **17 Suppl 4**, iv1–iv62 (2015).
12. Johnson, D. R. & O'Neill, B. P. Glioblastoma survival in the United States before and during the temozolomide era. *J Neurooncol* **107**, 359–364 (2012).
13. Campos, B., Olsen, L. R., Urup, T. & Poulsen, H. S. A comprehensive profile of recurrent glioblastoma. *Oncogene* (2016). doi:10.1038/onc.2016.85
14. Louis, D. N. *et al.* The 2007 WHO Classification of Tumours of the Central Nervous System. *Acta Neuropathol* **114**, 97–109 (2007).
15. Ellingson, B. M. *et al.* Probabilistic radiographic atlas of glioblastoma phenotypes. *AJNR Am J Neuroradiol* **34**, 533–540 (2013).
16. Gladwish, A. *et al.* Evaluation of early imaging response criteria in glioblastoma multiforme. *Radiat Oncol* **6**, 121 (2011).
17. Vredenburgh, J. J. *et al.* Bevacizumab plus irinotecan in recurrent glioblastoma multiforme. *J. Clin. Oncol.* **25**, 4722–4729 (2007).

18. Claes, A. *et al.* Magnetic resonance imaging-based detection of glial brain tumors in mice after antiangiogenic treatment. *Int. J. Cancer* **122**, 1981–1986 (2008).
19. Chamberlain, M. C. Bevacizumab for recurrent malignant gliomas: efficacy, toxicity, and patterns of recurrence. *Neurology* **72**, 772–3– author reply 773–4 (2009).
20. Ellingson, B. M. *et al.* Quantitative volumetric analysis of conventional MRI response in recurrent glioblastoma treated with bevacizumab. *Neuro-Oncology* **13**, 401–409 (2011).
21. Nicolasjilwan, M. *et al.* Addition of MR imaging features and genetic biomarkers strengthens glioblastoma survival prediction in TCGA patients. *J Neuroradiol* **42**, 212–221 (2015).
22. Zhou, M. *et al.* Radiologically defined ecological dynamics and clinical outcomes in glioblastoma multiforme: preliminary results. *Translational Oncology* **7**, 5–13 (2014).
23. Gutman, D. A. *et al.* MR imaging predictors of molecular profile and survival: multi-institutional study of the TCGA glioblastoma data set. *Radiology* **267**, 560–569 (2013).
24. Belden, C. J. *et al.* Genetics of Glioblastoma: A Window into Its Imaging and Histopathologic Variability. **31**, 1717–1740 (2011).
25. Shannon, C. E. & Weaver, W. *The Mathematical Theory of Communication*. (University of Illinois Press, 2015).
26. Huang, D. W., Sherman, B. T. & Lempicki, R. A. Systematic and integrative analysis of large gene lists using DAVID bioinformatics resources. *Nat Protoc* **4**, 44–57 (2009).
27. Ashburner, M. *et al.* Gene ontology: tool for the unification of biology. The Gene Ontology Consortium. *Nat. Genet.* **25**, 25–29 (2000).
28. Barbie, D. A. *et al.* Systematic RNA interference reveals that oncogenic KRAS-driven cancers require TBK1. *Nature* **462**, 108–112 (2009).
29. Murat, A. *et al.* Stem cell-related ‘self-renewal’ signature and high epidermal growth factor receptor expression associated with resistance to concomitant chemoradiotherapy in glioblastoma. *J. Clin. Oncol.* **26**, 3015–3024 (2008).